Infrared spectroscopic study of molecular hydrogen bonding in chiral smectic liquid crystals

Won Gun Jang, Cheol S. Park, K. H. Kim, Matthew A. Glaser, and Noel A. Clark
Ferroelectric Liquid Crystal Materials Research Center, Department of Physics, University of Colorado, Boulder, Colorado 80309-0390
(Received 2 May 2000)

We report the use of Fourier-transform infrared (IR) spectroscopy to probe intermolecular and intramolecular hydrogen bonding in thermotropic liquid-crystal phases. Infrared spectra of aligned smectic liquid crystal materials vs temperature, and of isotropic liquid-crystal mixtures vs concentration were measured in homologs both with and without hydrogen bonding. Hydrogen bonding significantly changes the direction and magnitude of the vibrational dipole transition moments, causing marked changes in the IR dichroic absorbance profiles of hydrogen-bonded molecular subfragments. A GAUSSIAN94 computation of the directions, magnitudes, and frequencies of the vibrational dipole moments of molecular subfragments shows good agreement with the experimental data. The results show that IR dichroism can be an effective probe of hydrogen bonding in liquid-crystal phases.

PACS number(s): 61.30.Gd, 78.30.Jw

I. INTRODUCTION

Hydrogen bonding (H bonding) is one of the key attractive interactions stabilizing condensed phases and promoting molecular self assembly. The directionality of H bonding gives rise to a variety of exotic material properties and phase behavior, ranging from the anomalous thermal expansion of water to the reentrant phase separation of many aqueous-organic binary mixtures. The effects of H bonding in liquid-crystal (LC) -forming materials is particularly interesting. For example, molecules incapable of mesogenic ordering can H bond into larger units that do have liquid crystal phases. Many studies of the role of H bonding in the formation and stabilization of liquid crystals have been carried out, ranging from the development of the classic smectic-*C* (Sm-*C*) phases formed from benzoic acid dimers [1], to more recent studies of the effects of inter- and intramolecular H bonding on LC phase stability [2,3]. H bonding impacts a variety of problems of current interest in LC science. For example, efforts have been recently made to utilize intramolecular H bonding to increase spontaneous ferroelectric polarization $\mathbf{P}_s$, in chiral smectic-*C** (Sm-*C**) phases [4], on the belief that H bonding would align the dipole moments of a carbonyl group and of a hydroxyl substituent on a phenyl ring into the same direction. In another recent study, LC-forming dimers having a bent (banana) shape have been prepared by complexation of phthalic or isophthalic acid and two molecules of stilbazole through intermolecular H bonding [5]. It has also been reported that the mesogen formed by the H bonding between chiral mono-(2-methylbutyl)-ester of terephthalic acid and 4-alkoxy-4′-stilbazole homologs has blue phases, the chiral nematic (*N**) phase, and the Sm-*C** phases [6]. Intermolecular bonding between H-bond donor and acceptor moieties has also been used to induce LC side chain polysiloxanes and to extend mesogens, producing more stable mesophases [7,8].

An especially powerful way of probing molecular ordering in LC phases is infrared dichroism: the orientational ordering of molecules in LCs makes the polarization dependence of the absorbance of infrared light by molecular vibrations an effective tool for probing molecular organization. In this paper, we use IR dichroism to study LCs in which there is H bonding, illustrating with a variety of examples that H bonding significantly alters the interpretation of IR dichroism data. We study-oriented preparations of several chiral smectic-*A** (Sm-*A**) and Sm-*C** liquid crystals, comparing the behavior of molecular homologs that differ only by the addition of a single H-bonding moiety. We probe the vibrational transition moment orientations of the phenyl rings, the C═O groups, and the H-bond-inducing OH and NH groups within molecules, as well as the molecular orientation and conformation distribution in the smectic phases. Temperature and concentration of H-bonding species are key parameters in these experiments, because H bonds can be expected to be broken thermally or by dilution of H-bonding molecules. Wave number shifts as well as changes in band intensity and shape are analyzed in terms of variations of intra- and inter-molecular H bonding [9]. Observed transition moment frequencies, directions and magnitudes are calculated using GAUSSIAN94 computational chemistry tools for comparison with the data.

II. EXPERIMENTS

IR dichroism

The experimental cell geometry is represented in Fig. 1. The LC samples were planar aligned in IR transparent capacitors made from CaF_2 windows coated with a 100-Å-thick layer of indium tin oxide for electrodes, and 200-Å-thick rubbed nylon alignment layers. The smectic phases were aligned into the bookshelf geometry, with the layers normal to the rubbing and normal or nearly normal to the plates, the latter induced by field application or by slow cooling from the isotropic. The spacing between the plates was $2<t<3$ μm, maintained by polyball spacers. IR light is incident normal to the cell plates and linearly polarized in the **y-z** plane at an angle Ω relative to the layer normal **z**, Ω being determined by a wire-grid IR polarizer oriented under computer control. Vibrational absorption peaks are background subtracted and fit, based on the Levenberg-Marquardt

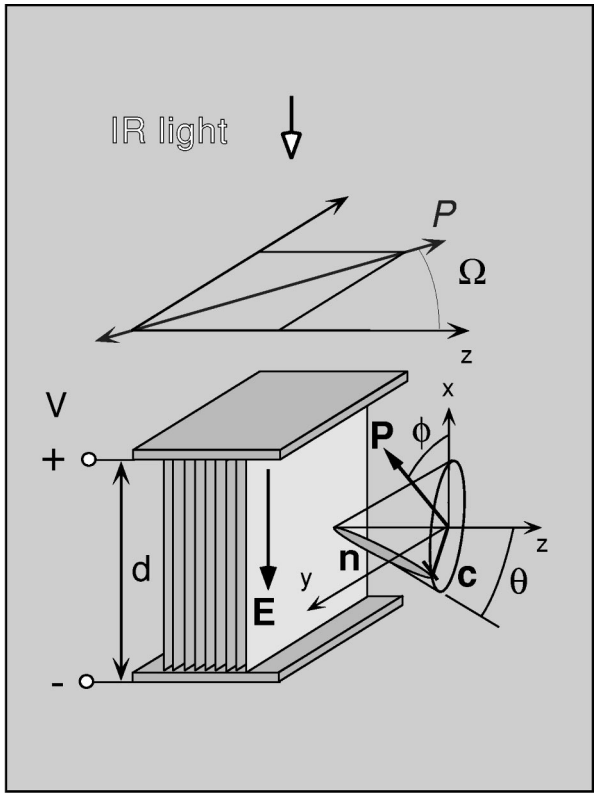

FIG. 1. A schematic diagram of the FTIR experiment.

algorithm, to a combination of Gaussian and Lorenzian functions to determine the peak absorbances of vibrations of interest [10].

In order to extract vibrational moment and molecular orientation parameters from IR dichroism data, it is necessary to measure absorbance versus polarizer orientation Ω for the full range of Ω [11,12]. Ignoring birefringence [13], $A(\Omega)$ for any mode is a universal function of three parameters, the absorbances A_{para} (A_{perp}) measured with the IR polarizer parallel (perpendicular) to the $\Omega_0=0$ axis, the polarizer orientation for either maximum ($A_{\max}$) or minimum ($A_{\min}$) absorbance

$$A(\Omega)=-\log\{(10^{-A_{\text{para}}})\cos^2(\Omega-\Omega_0)+(10^{-A_{\text{perp}}})\sin^2(\Omega-\Omega_0)\}. \quad (1)$$

Thus, Eq. (1) obtains for $A(\Omega)$ no matter what the molecular orientation distribution, with the three parameters $A_{\max}$, $A_{\min}$, and Ω_0 related to the three moments $\langle p_y^2\rangle$, $\langle p_z^2\rangle$, and $\langle p_y p_z\rangle$, of the absorption dipole **p**.

Liquid crystal materials

The ferroelectric liquid-crystal materials used in this study and their phase diagrams are shown in Fig. 2. The materials have been designed and synthesized in an effort to obtain ferroelectric Sm-*C** LCs, and, indeed, all of them have the Sm-*C** phase, as well as the Sm-*A**. The compounds NTT-noOH (materials provided by NIT, Inc., Japan, without OH) and NTT-OH [14] differ only by the lateral OH substitution on the core phenyl. NTT-OH has a very high $\mathbf{P}_s=-665$ nC/cm^2 at T=29 °C, whereas NTT-noOH has a

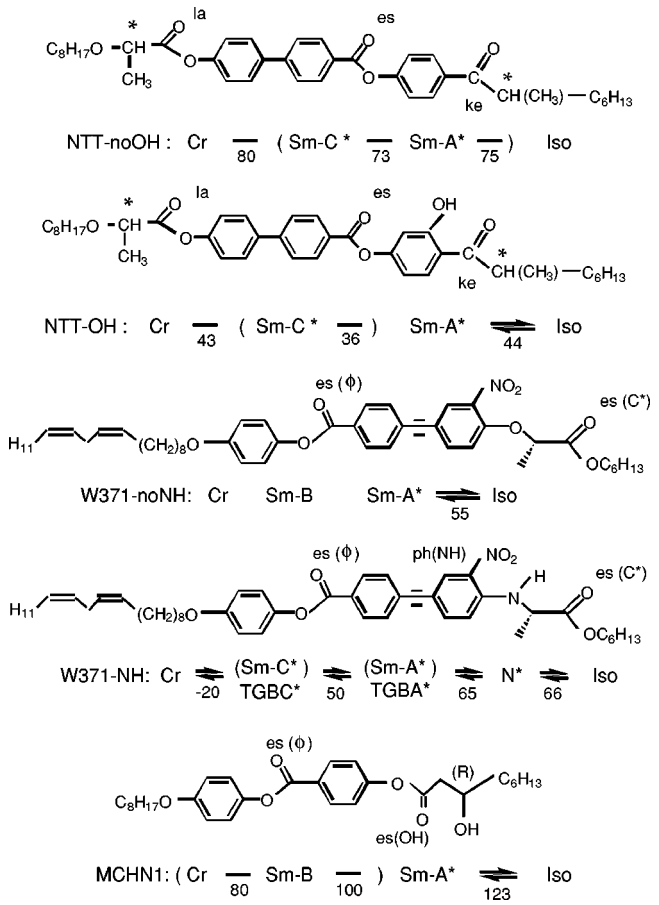

FIG. 2. Liquid crystal materials used in this experiments and their phase diagrams.

$\mathbf{P}_s=-512$ nC/cm^2. W371-NH (material provided by D. M. Walba, Dept. of Chemistry, University of Colorado at Boulder) was designed for large nonlinear susceptibility by introducing the NO_2 on the core phenyl and has a high Sm-*C** $\mathbf{P}_s=-19.7$ nC/cm^2 at 40 °C as a result of the NO_2 dipole. Because of the tolane group, the W371 family has a tendency to form twisted grain boundary (TGB) phases, with W371-NH having both twisted grain boundary *A* (TGBA) and twisted grain boundary *C* (TGBC). In the CaF_2 IR cells, application of a few volts unwinds the TGB helix and establishes bookshelf alignment [15]. W371-noNH has no Sm-*C* phase. MCHN1 (material provided by Mitsubishi, Inc., Japan) has Sm-*A* and Sm-*B* phases.

Dichroism experiments

In order to extract vibrational moment and molecular orientation parameters from IR dichroism data, $A(\Omega)$ was obtained by fits to the spectra for a series of Ω, spaced by 10° intervals over 360°. The results are displayed in Figs. 3–5 as polar plots of peak absorbance $A(\Omega)$, which effectively exhibit the dichroism of each mode.

NTT compounds

Figure 3 shows dichroism data $A(\Omega)$ of several molecular vibration bands of the two NTT compounds in the Sm-*A** phase ($T=39$ °C). These materials possess three C═O groups whose stretching vibrations are distinguishable in the IR spectra. The $A(\Omega)$ for these and the phenyl stretching peak are shown in Fig. 3 (ke, *keto carbonyl*; es, *ester carbo-*

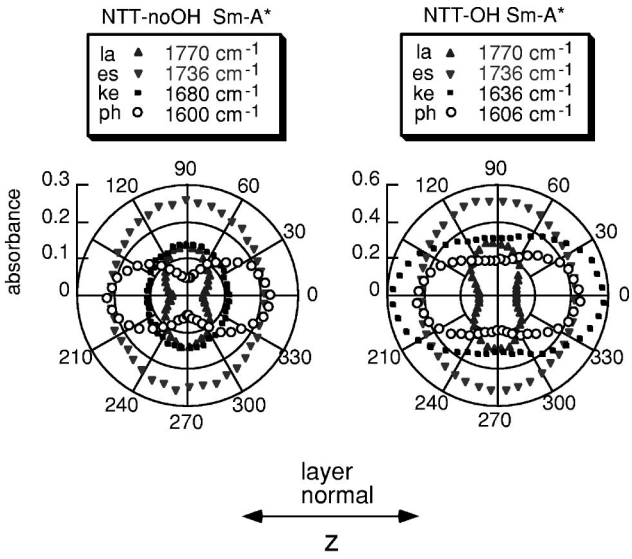

FIG. 3. Polar plot of absorption profiles for phenyl and C═O stretching vibrations in the NTT compounds. The keto (ke) C═O peak at 1636 cm^{-1} shows *abnormal* dichroism with the OH substitution on the phenyl ring, with maximum absorbance for polarization parallel to the layer normal. The lactic (la) and ester (es) C═O and phenyl (ph) absorbance data are also shown.

nyl; la, *lactic carbonyl*; ph, *phenyl*), where the different C═O groups are indicated in Fig. 2.

NTT-noOH. $A(\Omega)$ observed can be qualitatively understood for each mode in terms of β, the angle between its absorption dipole and the molecular long axis [12]. In NTT-noOH the phenyl core vibration has $\beta_{\text{phenyl}} \sim 0°$ and thus the largest change in absorbance [the dichroic ratio (D) is defined as $A_{\max}/A_{\min} \sim 4.25$ with maximum at $\Omega = 0°$]. The NTT-noOH carbonyl stretching vibrations, with β in the range $60° < \beta < 80°$, show behavior typical for non-H-bonded smectic-*A* materials [16,12]. They have a smaller dichroic ratio ($D < 2$) than the phenyl, and have $A_{\max}$ at $\Omega = 90°$, both because of the proximity of β to the ''magic angle'' $\beta = 54.7°$, for which a uniaxial distribution around the long axis appears isotropic ($D = 1$ for $\beta_{\text{magic}} = 54.7°$) and because $A_{\max}$ is at $\Omega = 90°(0°)$ for $\beta > (<) \beta_{\text{magic}}$. The la C═O has the largest $\beta(\beta_{\text{la(C=O)}} \sim 80°)$ and thus its D is the largest of the dichroic ratios of the carbonyls [12].

NTT-OH. NTT-OH exhibits a dichroism pattern that is similar to that of the NTT-noOH, with the exception of a dramatic difference for the ke C═O near the OH ($D_{\text{ke(C=O)}} = 1.86$). Specifically, the NTT compound *with* the OH group on the phenyl ring exhibits $A_{\max}$ for the ke C═O group at $\Omega = 0°$, rather than $\Omega = 90°$ for the NTT-noOH. Additionally, even though the molecular shape has hardly changed, the dichroic ratio of the phenyl stretching peak decreases to $D_{\text{ph}} = 2.31$, i.e., indicating either a decrease in order parameter or a reorientation of the absorption dipole relative to the long molecular axis, i.e., an increase of β_{ph}. Dichroism data for the OH stretching vibration was not possible to obtain because of the overlap with the CH stretching peaks.

W371 compounds

Remarkable IR dichroism behavior, illustrated in Fig. 4, was also observed for the C═O vibrations in the smectic-*A* phase of the W371 compounds, as follows.

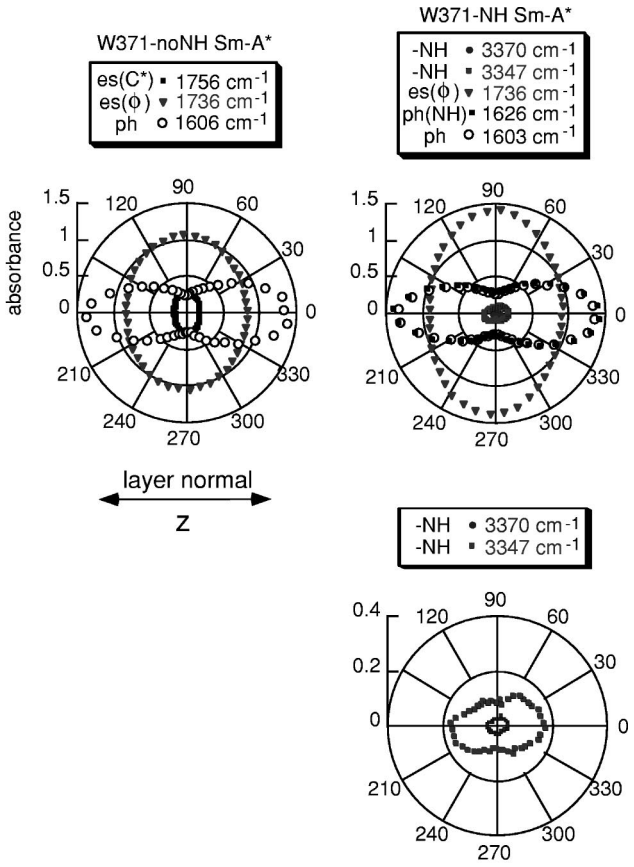

FIG. 4. Polar plot of absorption profiles of the W371 compounds. The 1756 cm^{-1} C═O peak disappears upon the introduction of NH, shifted down in wave number to overlap the 1736 cm^{-1} peak, increasing its dichroism.

W371-noNH. The carbonyl and phenyl absorbance profiles of W371-noNH look quite as expected, with A_{max} at $\Omega = 0°$ for the phenyl and at $\Omega = 90°$ for the es (ϕ) carbonyl at 1736 cm^{-1} and es (C^*) carbonyl at 1756 cm^{-1}.

W371-NH. In W371-NH, the peak from the es(C*) C═O group at 1756 cm^{-1} disappears, and small peaks appear at

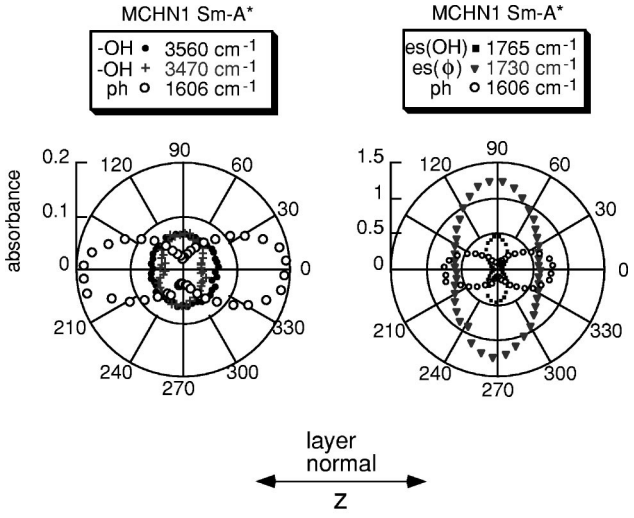

FIG. 5. Polar plot of absorbance of MCHN1. There are two OH peak frequencies, 3470 and 3560 cm^{-1}, for molecules with stronger and weaker H bonding, respectively.

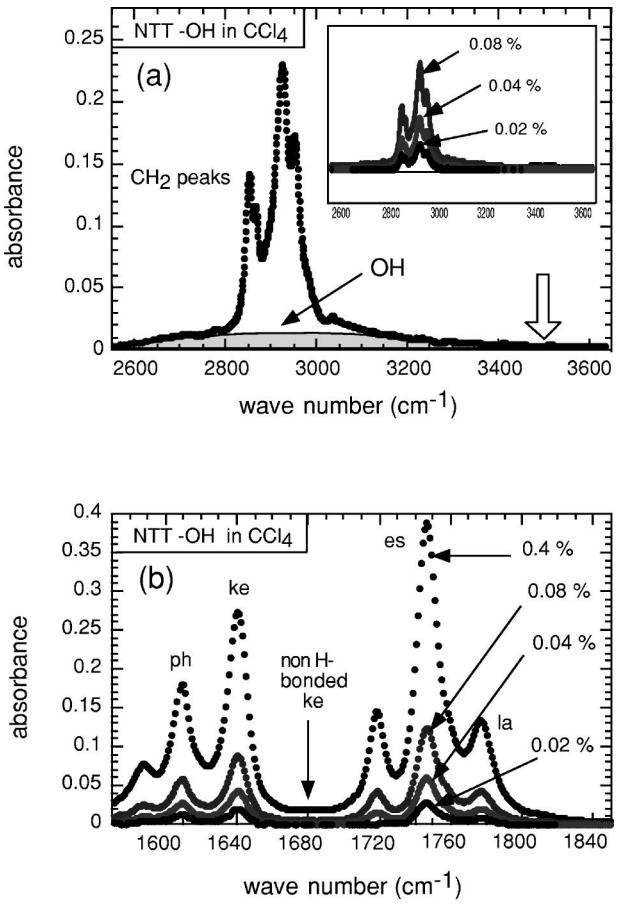

FIG. 6. Results of the dilution experiment for NTT-OH in CCl_4. (a) The OH peak with strong H bonding overlaps the CH_2 peaks. The non-H-bonded OH stretching peak, expected at the white arrow, is absent. (b) The C═O frequencies are independent of concentration, with frequencies indicating no H bonding for the es and la and strong H-bonding for the ke, the 1680 cm^{-1} non-H-bonded ke peak being absent.

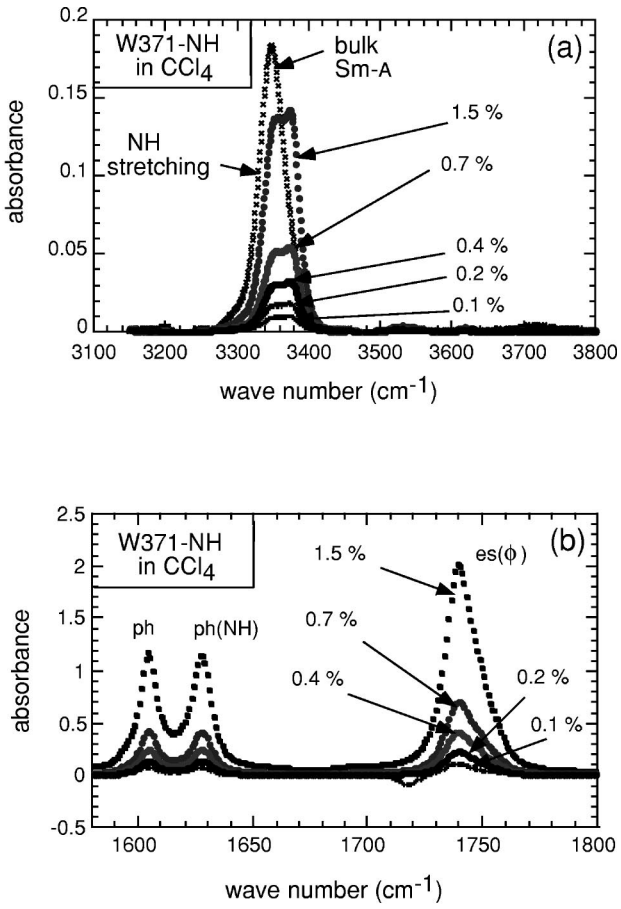

FIG. 7. Results of the dilution experiment for W371-NH in CCl_4. (a) The split NH peak indicates two kinds of H bonding: the strongly H-bonded NH peak at $\sim$3347 cm^{-1} and the weakly H-bonded NH stretching peak at $\sim$3370 cm^{-1}. (a, b) The concentration independence of NH and ph(NH) wave numbers indicates intramolecular H-bonding.

3370 cm^{-1} and 3347 cm^{-1} assignable to a H-bonded NH group. In addition, a high dichroic ratio peak ($D\sim4.91$ at 1626 cm^{-1}) with A_{max} at $\Omega=0°$ appears and the es (ϕ) C═O (1736 cm^{-1}) dichroic ratio apparently increases from $D_{es}=1.28$ to $D_{es}=1.53$.

MCHN1 compound

In smectic-*A* MCHN1, peaks from the two C═O groups were observed, es (ϕ) at 1730 cm^{-1} and es (OH) at 1765 cm^{-1}, a high dichroic ratio phenyl peak ($D_{ph}=7.87$), and also two small but distinct OH peaks (3470 cm^{-1} and 3560 cm^{-1}), having A_{max} at $\Omega=90°$, as illustrated in Fig. 5.

Dilution and temperature scan experiments

Dilution experiments for further study of H-bonding effects were carried out, dissolving the NTT-OH and W371-NH compounds at low concentration in carbon tetrachloride (CCl_4), which has no H-bonding interactions. MCHN1 did not readily dissolve in the available nonpolar, non-H-bonding solvents, so its H-bonding characteristics were studied by varying temperature, *T*. Results of these experiments are as follows.

NTT-OH. Particular attention was paid to the OH stretching peak, expected to have a wave number *k* in the region 2500 $cm^{-1}<k<2900$ cm^{-1} when H bonded, and $k\approx3500$ cm^{-1} when not H bonded [17]. The NTT-OH/CCl_4 spectra in Fig. 6 show no signal for $k\sim3500$ cm^{-1} no matter how much NTT-OH is diluted, but show a broad peak for $k\sim2900$ cm^{-1} overlapping the CH stretching peaks, not observed in absence of OH. This dilution experiment clearly shows that the OH group undergoes strong concentration independent, and therefore *intramolecular* H bonding, which can be only to the ke C═O. Consistent with this is the observation that the wave numbers of the three C═O groups, in particular the ke carbonyl, are not shifted at all upon dilution. Furthermore, the ke C═O stretching frequency is found at 1636 cm^{-1}, the frequency range expected when H bonded, and that there is no sign of a non-H-bonded ke carbonyl peak, expected at $k\approx1680$ cm^{-1} from the spectra of NTT-noOH.

W371-NH. Figure 7 shows spectra in the NH stretching region of W371-NH, both for the neat compound in the Sm-*A* phase, and under various conditions of dilution in CCl_4. The NH stretching frequency is expected to be 3340 cm^{-1} when H bonded and 3370 cm^{-1} when not H bonded [17].

The NH peak, at $k \approx 3340$ cm^{-1} in the neat Sm-*A*, is split in solution into two peaks, shifted up in wave number to $k \approx 3347$ cm^{-1} and $k \approx 3370$ cm^{-1}. These peak positions and relative intensities are independent of W371-NH concentration, indicating that there are two distinct modes of intramolecular H bonding in solution, the weaker giving the larger shift. The ph (NH) wave number is independent of concentration, also indicative of intramolecular H bonding. The es (ϕ) C═O wavenumbers are independent of concentration, as expected since this C═O is not involved with H bonding. In W371-NH, the es (NH)C═O stretching frequency is expected to be 1626 cm^{-1}.

MCHN1. *T* scans showed bimodal intensity distributions for both the OH and es (OH) C═O regions, with the low T wave numbers ($k_{OH} \approx 3440$ cm^{-1}, $k_{C=O} \approx 1735$ cm^{-1}) indicating an OH—C═O H bond. These peaks decrease and non-H-bonding peaks grow for both regions with increasing *T* (see Fig. 8).

Calculation of wave numbers and transition moments

In order to understand the dependence of the molecular structure and transition moment directions on H bonding, and to assist in assigning spectral features, we carried out density functional theory (DFT) calculations of vibration wave numbers and transition moment magnitudes and directions using GAUSSIAN94 [18,19]. In DFT, the total energy is a functional of the atomic electron density, expressed as basis set of functions. The basis set used here, 6-31G* [or 6-31G(d)], comprised of six Gaussian functions for the atomic core orbitals, and three inner and one outer Gaussian function for the atomic valence orbitals. The asterisk indicates that a set of *d* functions was added for each nonhydrogen (heavy) atom. Electron correlation was incorporated using the Becke3LYP (B3LYP) correlation functional, Becke's three-parameter hybrid variant of the Lee, Yang, and Parr correlation functional [20,21]. The CPU time requirements and performance of DFT calculations depend not only upon the size of the chemical system, but also upon the ''tightness'' of the integration grid, smaller grid spacing giving more accurate energies and electron density. Limits set by finite computational resources required calculations to be carried out only on fragments of the LC molecules. The fragments chosen were the smallest molecular entities incorporating all electrons having significant correlations with those of interest, and the grid spacing chosen for a particular molecular fragment was the smallest consistent with available CPU time. Relative energies of conformations of particular fragments were always compared with the same grid spacing [22]. Vibration frequencies and transition moments were calculated by GAUSSIAN94 with Ampac graphic interface. Calculated wave numbers were scaled by the factor 0.9613 appropriate for the B3LYP/6-31G* level [18].

Table I shows the calculated wave numbers for the vibrations under study along with experimental values obtained in the Sm-*A* phase of the neat compounds. The correlations between calculated and measured wave numbers is generally quite good, and reveals significant effects of H bonding, as discussed in the previous sections and below.

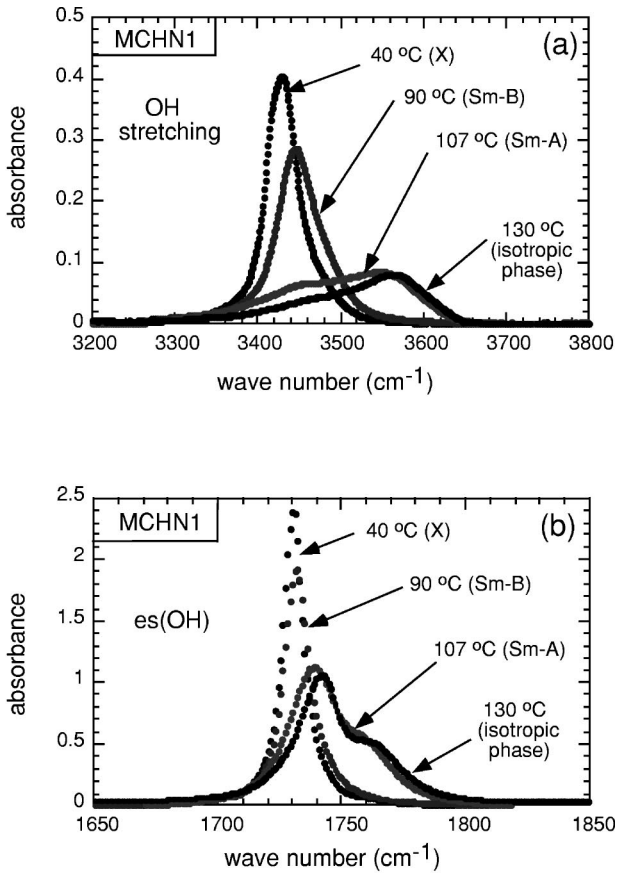

FIG. 8. Results of the temperature scan experiment of MCHN1. Both the OH and es(OH) peaks show evidence for a *T*-dependent OH—C═O H-bond, evolving from H-bonded wave numbers at low *T* (3440 and 1740 cm^{-1}, respectively) to split peaks at high T, with non-H-bonded peaks (3560 and 1765 cm^{-1}) appearing.

III. DISCUSSION

NTT compounds

The most striking observation in the NTT compound spectra was the 90° change in the Ω of A_{min} in $A(\Omega)$ of the ke carbonyl upon introduction of the OH phenyl ring substitution. This change indicates that the dipole transition moment direction of ke C═O is rotated significantly (by more than 30°) *toward* the molecular long axis upon H bonding. Additionally, the vibration wave number of this carbonyl undergoes a big shift, from 1680 cm^{-1} to 1636 cm^{-1} and the dichroic ratio of the phenyl peak (1606 cm^{-1}) decreases to *D* of the 1606 cm^{-1} peak to ~ 2.31. These changes can be understood on the basis of the computed transition moments in the NTT compounds' molecular fragments shown in Fig. 9. The vibration wave number calculation yields a ke carbonyl wave-number shift from 1697 cm^{-1} (-noOH) to 1638 cm^{-1} (with OH), and a change in the transition moment direction to $\beta_{C=O} = 25°$, for which we expect $D = 2.73$ [11] and A_{max} for $\Omega = 0°$, as observed. The two es carbonyl frequencies are independent of the presence of the OH group para to the ester, in agreement with experiments.

The phenyl group frequencies are not changed by the presence of the OH, in agreement with experiments. Furthermore, the calculated β_{phenyl} increases to $\beta_{phenyl} = 45°$, which is responsible for the decrease of the D_{1606} of the

TABLE I. Experimental and calculated wave numbers (cm^{-1}).

		Experimental	Calculated
	NTT compounds		
Keto C═O (ke)	without OH	1680	1697
	with OH	1636	1638
Ester C═O (es)	without OH	1736	1742
	with OH	1736	1745
Lactic C═O (la)	without OH	1770	1760
	with OH	1770	1760
OH	without OH	NA	NA
	with OH	2900	3137
Phenyl (ph)	without OH	1600	1594
	with OH	1606	1605
	W371 compounds		
Ester C═O (es)	without NH	1736	1736
	with NH	1736	1736
Ester C═O [es(C*)]	without NH	1756	1763
	with NH	1736	1745
NH	without NH	N/A	N/A
	with NH	3347	3351
		3370	3367
Phenyl (ph)	without NH	1600	1600
	with OH	1600	1605
Phenyl [ph(NH)]	without NH	1560	1549
			1570
	with NH	1626	1617
	MCHN1 compound		
Ester C═O [es(OH)]	with H-bond	1730	1722
	without H-bond	1765	1758
OH	with H-bond	3470	3560
	without H-bond	3560	3571
Phenyl (ph)	with H-bond	1600	1600
	without H-bond	1600	1605

1606-cm^{-1} peak. $\beta_{\text{phenyl}}=45°$ yields a $D_{\text{phenyl}}=1.6$ for the absorbance of the phenyl which, when added to the absorbance of the biphenyl ($D_{\text{biphenyl}}=4.25$ from the NTT-noOH data), yields a decrease in the apparent D of the 1606 cm^{-1} peak to $D_{1606}=2.8$, as shown in Fig. 10. This is close to the observed $D_{1606}=2.31$.

The computation results of the vibrational wave number of the OH group are also reasonably consistent with experiments, showing no peak around 3500 cm^{-1}, rather a significant downshift to 3137 cm^{-1}, compared with the experimental value of around 2900 cm^{-1}. This indicates that strong H bonding exists, as already found in the dilution experiments. Thus, the dichroism and dilution experiments and the computations all indicate an OH—ke C═O *intramolecular* H-bond that is strong enough not to be broken by any dilution or temperature increase.

W371 compounds

The W371 compounds also exhibit very interesting behavior upon introduction of the NH group. The 1756 cm^{-1} C═O peak disappears and NH peaks (3370 and 3347 cm^{-1}) and a new 1626 cm^{-1} peak with high $D_{1626}\sim 4.91$ appear. We also note that the 1736 cm^{-1} C═O dichroic ratio increases considerably from $D_{1736}\sim 1.28$ to $D_{1736}\sim 1.53$.

These effects can be largely accounted for by the calculations. Figures 11(a) and 11(b) show the calculated low-energy conformations of the molecular fragments used to model H bonding in the chiral tail of W371-NH. The intermolecular distance between H of NH and O of NO_2 was 1.84 Å in the optimized structure of W371 [see Figs. 11(a) and 11(b)], which is in the range of effective H bonding (1.8 to 2.2 Å), and the energetics of distortion indicate a strong

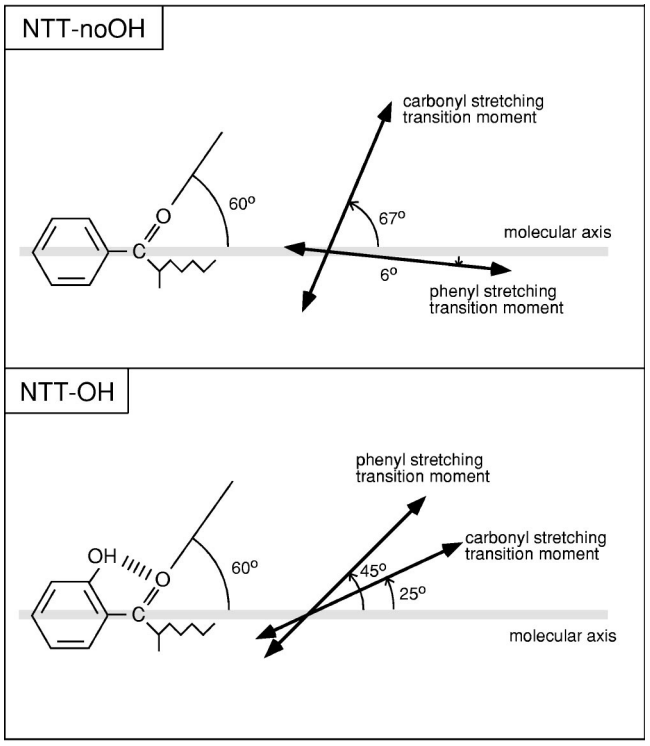

FIG. 9. Transition moment directions calculated for NTT-OH and NTT-noOH fragments, showing the effect of the OH substitution and OH—C═O H-bonding. (a) The noOH orientations are quite typical. (b) H-bonding shifts the transition moment direction of the C═O stretching mode dramatically toward the molecular long axis. The phenyl stretching transition moment direction rotates away from the molecular axis.

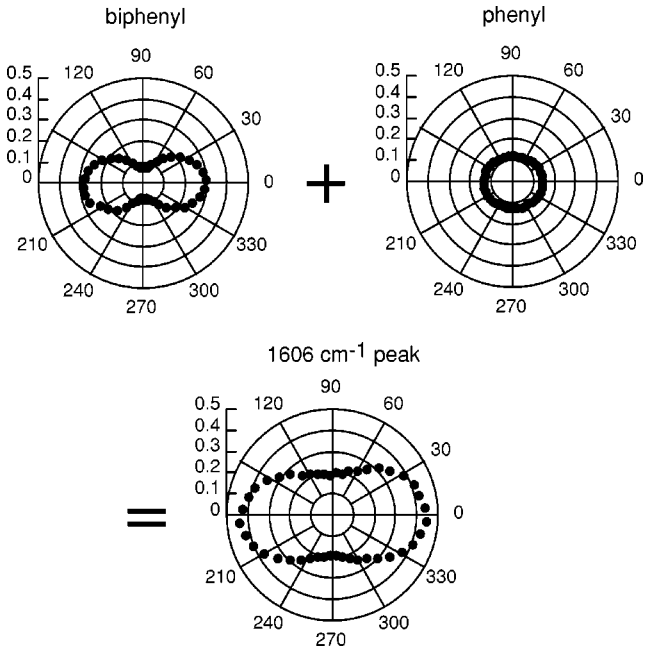

FIG. 10. The 1606-cm^{-1} profile in the NTT-OH is the sum of biphenyl ($D\sim4.25$) profile and single phenyl profile which undergoes the H bonding ($D\sim1.6$).

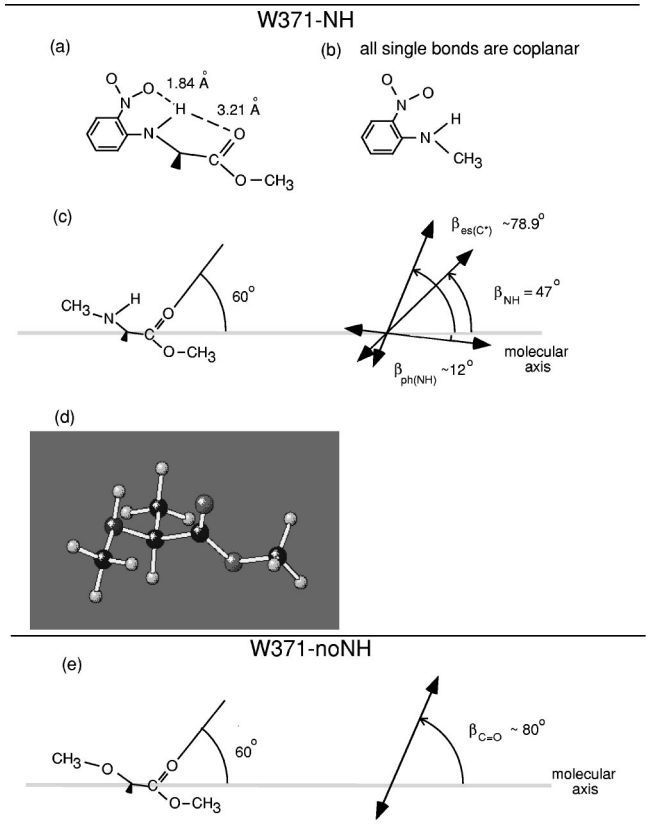

FIG. 11. Transition moment directions calculated for W371-NH and W371-noNH fragments, showing the effect of the NH substitution and NH—C═O H bonding. (a, b) Energetically favorable NO_2, NH conformation. These interatomic distances yield a strong NO_2-NH H-bond and weak C═O—NH H-bond. (c) Transition moment directions and magnitudes for the C═O ($|\mathbf{p}|_{C=O}=0.233$ Debye) and NH ($|\mathbf{p}|_{NH}=0.005$ Debye) groups for this fragment. (d, e) A low-energy conformation for a W371-noNH fragment. With C═O transition moment direction and magnitude ($|\mathbf{p}|_{C=O}=0.237$ Debye).

(~10kcal/mole) NO_2-NH hydrogen bond. Figure 11(c) indicates the transition moment magnitudes and directions of the C═O and NH stretching vibrations in the low-energy conformation of the chiral tail. The amino proton is 3.21 Å away from the carbonyl oxygen, close enough for a weak NH—C═O H-bonding interaction. The calculations predict a resulting downshift in the C═O stretching vibration frequency from 1763 to 1745 cm^{-1}. This downshift may account for the disappearance of the 1756 cm^{-1} es (NH) C═O peak upon introduction of the NH: weak H bonding reduces its frequency to $k\sim1736$ cm^{-1}, so that it overlaps the es C═O peak and increases its apparent dichroic ratio. As indicated in Fig. 12, the high dichroic ratio of the es (NH) C═O peak ($D_{es(NH)}\sim3.5$) adds together with the low dichroic ratio of the es C═O peak ($D_{es}\sim1.28$), giving rise to a final $D\sim1.72$.

The NH transition dipole of the NH stretching modes at 3347 and 3370 cm^{-1} (3351 and 3367 cm^{-1} from GAUSSIAN94) is calculated to have $\beta_{NH}=47°$, predicting a $D_{NH}=1.6$ with A_{max} at $\Omega_0=0°$, which compares to the measured $D_{NH}=1.9$ and 1.4. The calculations showed that the phenyl with the NO_2 substituent H-bonded to the NH exhibits

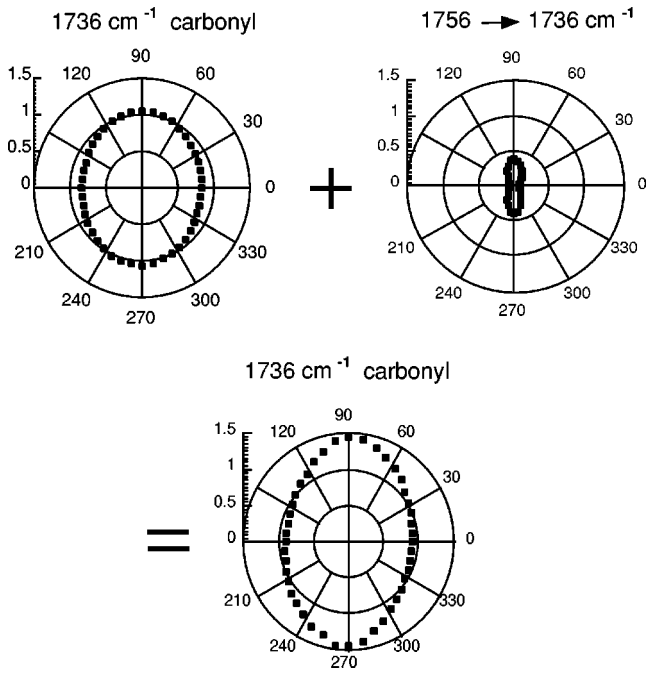

FIG. 12. The 1736−cm^{-1} C═O profile in the W371 compound is the sum of the es C═O ($D\sim1.28$) and es (NH) C═O profile, shifted in wave number from 1756 to 1736 cm^{-1} by H bonding.

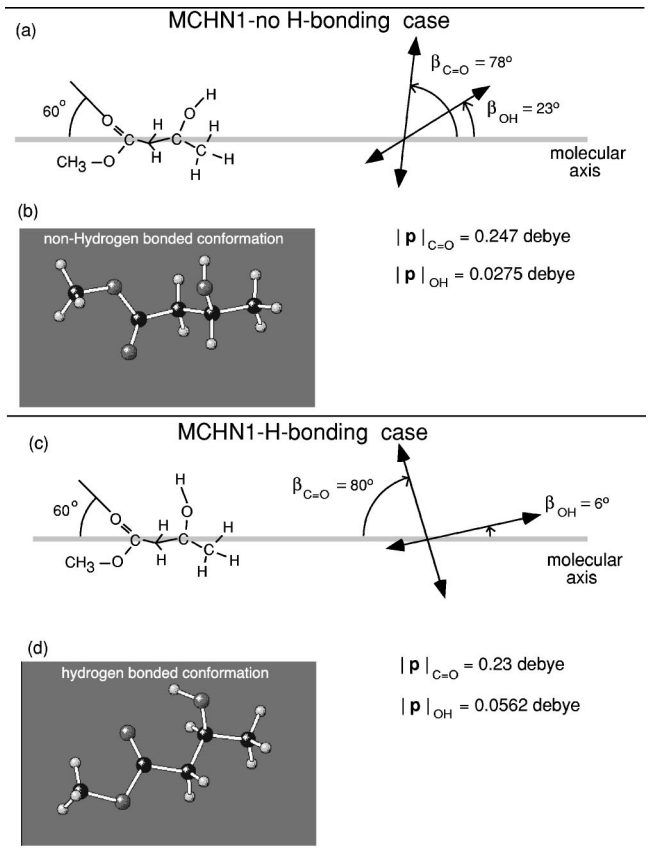

FIG. 13. Transition moment directions calculated for a MCHN1 fragment, showing the effect of OH—C═O H bonding.

coupled phenyl-NO_2-NH stretching modes at 1549, 1570, and 1617 cm^{-1}($|\mathbf{p}|=0.2$, 0.065, and 0.17 Debye, respectively). Peaks are observed at 1560 cm^{-1} and 1626 cm^{-1}. The 1626 cm^{-1} peak is large with $A_{\max}$ for $\Omega_0=0°$ and a large dichroic ratio $D_{1626}\sim4.91$. This value of D is consistent with the small $\beta_{\mathrm{ph(NH)}}=12°$, calculated for this coupled phenyl-NH vibration.

From the dilution experiment, whose results are shown in Fig. 7, we also know that there is H bonding, that is, weak H bonding for the NH group (3370 cm^{-1}) and for the carbonyl group (1756→1736 cm^{-1}). Initially weak H bonding is readily breakable from 3340 to 3370 cm^{-1} as dilution continues, but the strong H-bonded NH wave number remains unchanged (3347 cm^{-1}) from the liquid-crystal phase ($\sim$3340 cm^{-1}). Therefore, the 3347 and 3370 cm^{-1} relative peak intensities remain the same upon dilution because the portion of strong hydrogen-bonded NH and weak hydrogen-bonded NH remain unchanged, and consequently, dilution just changes the average intermolecular distances.

MCHN1 compound

Calculations for the magnitudes and directions of the transition moment of the C═O and OH stretching vibrations in the MCHN1 compound are also shown in Figs. 13. Figure 8 indicates that the H-bonded OH stretching peak wave number (3430 cm^{-1}) shifts up to 3450 cm^{-1} in the Sm-*B* phase and that the peak splits in the Sm-*A* phase, with a second peak appearing at 3560 cm^{-1}, a trend enhanced upon passage into the isotropic phase and indicative of a shift to higher wave number with weaker H bonding. The calculations also yield a shift to higher wave number with weaker H bonding, consistent with the observed behavior, although the calculated shift is smaller than the observed. The wave number of the es (OH) C═O ($k_{\mathrm{es(OH)}}\sim1765$ cm^{-1}) is indicative of weak OH—C═O bonding.

The calculated transition moments, shown in Fig. 13, do not change much in orientation upon H bonding, so the D data do not provide much information about the state of H bonding. The calculated large $\beta_{\mathrm{es(OH)}}\sim80°$ of the es (OH) C═O (1765 cm^{-1}) is consistent with the high observed $D_{\mathrm{es(OH)}}=3$–4, but this is quite a typical value for a phenyl-O-C═O conformation. The high D of es (OH) C═O (1765 cm^{-1}) is consistent with the calculated large $\beta_{\mathrm{es(OH)}}=80°$. The $D=2.11$ of es C═O peak at 1730 cm^{-1} is somewhat larger than that typically observed for es carbonyls ($D\sim1.3$). This is probably due to the subset of molecules in which the es(OH) C═O is strongly H-bonded, downshifting its wave number to 1730 cm^{-1} and overlapping the es peak. Since $\beta_{\mathrm{es(OH)}}$ is large, this overlap increases the D in the same way as shown in W371-NH in Fig. 12. The calculations have the transition moment of the OH stretching vibration nearly parallel to the molecular long axis ($\beta_{\mathrm{OH}}<25°$), predicting $A_{\max}$ at $\Omega=0°$, in disagreement with the data that show essentially no dichroism ($D_{\mathrm{OH}}\sim1$, $\beta_{\mathrm{OH}}=\beta_{\mathrm{magic}}=54.7°$), for the H-bonded OH peak and $A_{\max}$ at $\Omega=90°$ for the non-H-bonded OH peak ($\beta_{\mathrm{OH}}>\beta_{\mathrm{magic}}=54.7°$), although the increase in β_{OH} upon H bonding is the same in both cases.

IV. SUMMARY

In this study, we have presented and analyzed LC materials with several distinct kinds of intramolecular H bonding. Our principal conclusion is that currently available quantum chemical calculational tools, such as GAUSSIAN94 and GAUSSIAN98, are effective for interpreting infrared dichroism experiments in organic systems with orientational ordering of H-bonded groups. The effects of H bonding on the vibrational transition moments are quite significant, making FTIR an effective means of studying such systems.

ACKNOWLEDGMENT

This work was supported by NSF MRSEC Grant No. DMR 98-09555.

[1] R.F. Bryan, J. Chem. Soc. **1967**, 2517; J. S. Dave and R. A. Vora, *Liquid Crystals and Ordered Fluids* (New York, Plenum 1970) Vol. **S. 477**; Ju. Amerik and B.A. Krentsel, J. Polym. Sci. **16**, 1383 (1967).

[2] M. Pfaadt, G. Moessner, D. Pressner, S. Valiyaveettil, C. Boeffel, K. Mullen, and H.W. Spiess, J. Mater. Chem. **5**, 2265 (1995).

[3] C.M. Paleos and D. Tsiourvas, Reviews Angew. Chem. Ed. Engl. **34**, 1696 (1995).

[4] S. Ishibashi and S. Kobayashi, Liq. Cryst. **10**, 715 (1991).

[5] T. Kato, H. Adachi, A. Fujishima, and J.M. Frechet, Chem. Lett. **2**, 265 (1992).

[6] L.J. Yu, Liq. Cryst. **14**, 1303 (1993).

[7] U. Kumar, T. Kato, and J.M.J. Frechet, J. Am. Chem. Soc. **114**, 6630 (1992).

[8] T. Kato, T. Uryu, F. Kaneuchi, C. Jin, and J.M.J. Frechet, Liq. Cryst. **14**, 1311 (1993).

[9] A. Ghanem and C. Noel, Mol. Cryst. Liq. Cryst. **150b**, 447 (1987).

[10] Bruker FT-IR Reference manual OPUS/IR, Version 2.0.

[11] F. Hide, N.A. Clark, K. Nito, A. Yasuda, and D.M. Walba, Phys. Rev. Lett. **75**, 2344 (1995).

[12] W.G. Jang, C.S. Park, J.E. Maclennan, K.H. Kim, and N.A. Clark, Ferroelectrics **180**, 213 (1996).

[13] Equation 1 is exact only in absence of birefringence (optical anisotropy in the real part of the dielectric constant), when the eigenmodes of a dichroic medium are linearly polarized along the directions of maximum and minimum absorbance. For the vibrations studied here, polarized nearly along the optic axis of the real part of the dielectric constant, the birefringence can be ignored in few micron thick samples.

[14] S. Kobayashi and S. Ishibashi, Mol. Cryst. Liq. Cryst. **220**, 1 (1992); **257**, 181 (1994); K. Takahashi, S. Ishibashi, and S. Kobayashi, J. Am. Chem. Soc. **209**, 177 (1995).

[15] R. Shao, J. Pang, N.A. Clark, J.A. Rego, and D.M. Walba, Ferroelectrics **147**, 255 (1993).

[16] K.H. Kim, K. Ishikawa, H. Takezoe, and A. Fukuda, Phys. Rev. E **51**, 2166 (1995).

[17] N.B. Colthup, L.H. Daly, and S.E. Wiberley, *Introduction to Infrared and Raman Spectroscopy* (Academic Press, New York, 1964).

[18] *Gaussian94 User's Reference* (Gaussian, Inc., Pittsburgh, PA, 1995).

[19] *Exploring Chemistry with Electronic Structure Methods*, 2nd Edition, J. B. Foresman and A. Frisch (Gaussian, Inc., Pittsburgh, 1996).

[20] C. Lee, W. Yang, and R.G. Parr, Phys. Rev. B **37**, 785 (1988).

[21] A.D. Becke, Phys. Rev. A **38**, 3098 (1988), and references therein.

[22] M. Nendel, Ph.D. dissertation, University of California, Los Angeles, 1996 (unpublished).